# Multi-response optimization of process parameters during friction stir welding of AA2014-AA7075 using TOPSIS Approach

P. UMAMAHESWARRAO*

*Corresponding author
Department of Mechanical Engineering, Bapatla Engineering College,
Bapatla, A.P. India,
maheshponugoti@gmail.com

DOI: 10.13111/2066-8201.2023.15.1.10

*Received: 05 October 2022/ Accepted: 30 January 2023/ Published: March 2023*
Copyright © 2023. Published by INCAS. This is an "open access" article under the CC BY-NC-ND license (http://creativecommons.org/licenses/by-nc-nd/4.0/)

***Abstract:*** *In this study, multi-objective optimization for Friction stir welding of dissimilar AA2014-AA7075 has been presented to provide optimum tensile strength, hardness, and % of elongation. The input parameters considered for the analysis are tool rotational speed, feed, and tilt angle. Experiments are designed based on Taguchi $L_9$ orthogonal array. Investigative analysis on the effect of input parameters on the responses is carried out using the MINITAB14 software package. The parametric influence on responses is discussed through the main effects plot. Further, multi-objective optimization is performed with the Technique for order of preference by similarity to ideal solution (TOPSIS). Results demonstrated that tool rotational speed is the most significant factor affecting the response followed by feed and tilt angle. The optimum cutting parameters obtained are tool rotational speed 710 rpm, Feed 30 mm/rev, and Tilt angle 2$^o$.*

***Key Words:*** *Friction stir welding, Tensile strength, Hardness, TOPSIS, ANOVA*

## 1. INTRODUCTION

The 2XXX (Cu alloy) and 7XXX (Zn alloy) aluminium alloy series are high-strength, heat-treatable alloys that can be used in the aerospace sector [1]. High-strength alloys AA7075 and AA2014 are both often utilized in the aerospace sector; AA7075 is used to make upper wing components, floors, and body stiffeners, while AA2014 is frequently employed in aircraft structures [2-3]. As the maximum temperature during welding is in the range of 0.60 to 0.95 times the melting point of base metal, FSW is widely used in a variety of industrial sectors, including aerospace, automotive, shipbuilding, railway, and marine [4-11].

Because the physical, chemical, and mechanical properties of the two alloys to be joined are dissimilar, joining dissimilar alloys is challenging [12-15]. The aerospace, rail, automotive, and shipbuilding industries have been urged to use this technique for combining dissimilar aluminium alloys due to the growing demand for dissimilar joints and various benefits of the FSW process [1].

Chanakyan et al. [16] optimized process parameters by utilizing the grey relation analysis in friction stir welding of 5052 aluminium alloy. Results revealed that tool rotational speed and traverse speed are the most prominent parameters for multiple performance characteristics.

Nidhi Sharma et al. [17] investigated the influence of welding process parameters on ultimate tensile strength and micro-hardness during the joining of Al-6101 and pure copper. It is discovered that the two main process variables affecting tensile strength and micro-hardness are rotational speed and welding speed. Raj Kumar et al. [18] carried out multi-response optimization of process parameters by the desirability function approach in FSW of AA2014 and AA7075 dissimilar alloys. Optimal parameters were determined as welding speed 60 mm/min and rotary speed 1000 rpm to produce defect-free welded joints.

Farzadi et al. [19] studied the effect of operational parameters on ultimate tensile strength during friction stir welding of AA7075 aluminum alloy. It was concluded that UTS was most significantly influenced by the welding speed. The optimal process parameters are rotation speed of 380–530 rpm, the welding speed of 90–95 mm/min, the shoulder diameter of 14.2–17.8 mm, and the pin diameter of 5–6 mm.

The impact of different welding process parameters on the mechanical properties of AA6061 T6 and AA7075 T651 aluminium alloys during dissimilar welding was investigated by Madhusudan Manjunath et al. [20]. Conical and cylindrical tool pin profiles are used in this study to carry out the welding process. Results demonstrated that in contrast to conical tools, cylindrical tools have better tensile and elongation properties.

Ravi Sankar and Umamaheswarrao [21] optimized process parameters during friction stir welding of AA 6061 using the response surface method coupled with GRA and PCA. 800 rpm welding speed, 50 mm/min rotational speed, and a 4 mm tool diameter were the optimal process factors. The impact of process parameters and tool pin profile on the mechanical characteristics of AA2014 weldments was researched by Suvarna Raju et al. [22]. Results revealed that the better mechanical properties were obtained by using taper cylindrical threaded profile compared to straight cylindrical threaded pin.

Using the response surface method, Ravi Sankar and Umamaheswarrao [23] modelled and optimised the friction stir welding of AA 6061. The results showed that Tensile strength was higher at lower speeds; the joint's hardness initially rises and then falls as speed increases. Janusz Torzewski et al [24] analyzed the influence of process parameters on the micro hardness, and mechanical properties during FSW of dissimilar aluminum alloys 7020-T651 and 5083-H111. In all heat-affected zones, it was found that the base materials' hardness remained unchanged for both alloys and the three profiles.

Numerous investigations have been done on the 2xxx and 7xxx series alloys, but especially few have been done on the dissimilar welds of AA2014 and AA7075. Moreover, a systematic study on the effect of tool rotational speed, feed and tilt angle in dissimilar welds of AA2014 and AA7075 was not carried out. Hence the present work is aimed to determine the optimal welding parameters using TOPSIS.

## 2. EXPERIMENTAL DETAILS

The rolled plates of aluminum alloy AA2014 and AA7075 of 6 mm thick are cut into the required sizes (100 mm×75 mm) by a power hacksaw machine and a square butt configuration is prepared. Initial joint configuration was obtained by securing plates in position using mechanical clamps. The non-consumable tool made of H13 steel was used in the weld joint preparation. To carry out the FSW process, a vertical milling machine is employed. The work holding fixture was designed and tested before the experiments. The experimental setup is shown in Fig. 1. The FSW tool consists of a cylindrical cross-section of 19 mm shoulder diameter, while the tool pin thickness is 6 mm., and the length of the probe is 5.6 mm., as shown in Fig. 2. Tensile specimens were prepared as per ASTM-E8 standard. The chemical

composition of AA2014 and AA7075 is given in Table 1. Table 2 lists the process parameters and their levels. Table 3 displays the experimental results. Tensile test sample and hardness test samples are shown in Fig. 3 and Fig. 4, respectively.

Fig. 1 Experimental setup

Fig. 2 FSW tool

Fig. 3 Tensile test specimen sample

Fig. 4 Hardness test specimen sample

Table 1. Chemical composition of AA2014 and AA7075

| Alloy | Chemical composition (wt%) | | | | | | | |
|---|---|---|---|---|---|---|---|---|
| | Si | Fe | Cu | Mn | Mg | Cr | Zn | Al |
| AA2014 | 0.52 | 0.37 | 4.71 | 0.86 | 0.25 | - | - | Bal. |
| AA7075 | - | 0.32 | 1.56 | - | 2.26 | 0.22 | 6.25 | Bal. |

Table 2. Process parameters and their levels

| Parameter | Units | Level 1 | Level 2 | Level 3 |
|---|---|---|---|---|
| Tool rotational speed | rpm | 710 | 900 | 1120 |
| Feed | mm/rev | 30 | 40 | 50 |
| Tilt angle | $^{o}$ | 0 | 1 | 2 |

## 3. METHODOLOGY

### Technique for Order Preference by Similarity to Ideal Solution (TOPSIS)

TOPSIS was evolved by Hwang and Yoon based on the concept that the chosen parameter should have the shortest distance from the best solution and the longest distance from the worst solution [25]. In the TOPSIS approach, specific weight is given to output responses in order to rank them. The steps involved in the TOPSIS are given below.

Table 3. Experimental matrix along with results

| Expt. No | Tool rotational speed (rpm) | Feed (mm/rev) | Tilt angle ($^{o}$) | Ultimate Tensile Strength (N/mm$^2$) | Hardness | Percentage of Elongation |
|---|---|---|---|---|---|---|
| 1 | 710 | 30 | 0 | 275.107 | 116.33 | 3.380 |
| 2 | 900 | 50 | 0 | 171.238 | 104.33 | 0.740 |
| 3 | 1120 | 40 | 0 | 251.982 | 103 | 1.840 |
| 4 | 1120 | 50 | 1 | 245.483 | 112.33 | 2.16 |
| 5 | 710 | 50 | 2 | 264.282 | 111 | 2.460 |
| 6 | 710 | 40 | 1 | 238.481 | 103.33 | 3.22 |
| 7 | 900 | 30 | 1 | 252.780 | 105.67 | 2.8 |
| 8 | 900 | 40 | 2 | 244.292 | 93.9 | 2.62 |
| 9 | 1120 | 30 | 2 | 260.306 | 105.67 | 3.22 |

STEP 1

In the TOPSIS, the units of all criteria are eliminated and it has been converted into normalized value.

The normalized value ($r_{ij}$) is obtained using equation (1). The normalized performance values and weighted normalized values are shown in Tables 4 and 5.

$$r_{ij} = \frac{X_{ij}}{\sqrt{\sum_{i=1}^{m} X_{ij}^2}} \qquad i = 1, 2, 3 \ldots\ldots 32; \quad j = 1, 2, 3 \tag{1}$$

$i$ = number of alternatives (trials)

$j$ = number of criteria (Output responses)

$X_{ij}$= represents the actual value of the $i^{th}$ value of $j^{th}$ experimental run.

Table 4. Normalized Performance Value

| Expt. No | Tensile strength | Hardness | Percentage of Elongation |
|---|---|---|---|
| 1 | 5.860048 | 3.763251 | 0.713531 |
| 2 | 3.647536 | 3.375053 | 0.156217 |
| 3 | 5.367463 | 3.332028 | 0.388431 |
| 4 | 5.229028 | 3.633852 | 0.455984 |
| 5 | 5.629465 | 3.590826 | 0.519316 |
| 6 | 5.079878 | 3.342703 | 0.679755 |
| 7 | 5.384461 | 3.418402 | 0.591091 |
| 8 | 5.203658 | 3.037645 | 0.553092 |
| 9 | 5.544772 | 3.418402 | 0.679755 |

Table 5. Weighted Normalized Value

| Expt. No | Tensile strength | Hardness | Percentage of Elongation |
|---|---|---|---|
| 1 | 1.933815 | 1.241872 | 0.235465 |
| 2 | 1.203687 | 1.113767 | 0.051551 |
| 3 | 1.771262 | 1.099569 | 0.128182 |
| 4 | 1.725579 | 1.199171 | 0.150474 |
| 5 | 1.857723 | 1.184972 | 0.171374 |
| 6 | 1.676359 | 1.103092 | 0.224319 |
| 7 | 1.776872 | 1.128072 | 0.195060 |
| 8 | 1.717207 | 1.002422 | 0.182520 |
| 9 | 1.829774 | 1.128072 | 0.224319 |

STEP 2

The weighted normalized value ($v_{ij}$) is computed by multiplying the normalized value by its accompanying weights and is shown in equation (2),

$$v_{ij} = w_j \times r_{ij} \qquad i = 1, 2, 3 \ldots 32; \quad j = 1, 2, 3 \tag{2}$$

Here, equal weightage is given to all responses [26]. Therefore, $w_j = 0.33$.

Table 6. Positive ideal and Negative ideal solutions

| Expt. No | Tensile strength | Hardness | Percentage of Elongation |
|---|---|---|---|
| 1 | 1.93382 | 1.24187 | 0.23547 |
| 2 | 1.20369 | 1.11377 | 0.05155 |
| 3 | 1.77126 | 1.09957 | 0.12818 |
| 4 | 1.72558 | 1.19917 | 0.15047 |
| 5 | 1.85772 | 1.18497 | 0.17137 |
| 6 | 1.67636 | 1.10309 | 0.22432 |
| 7 | 1.77687 | 1.12807 | 0.19506 |
| 8 | 1.71721 | 1.00242 | 0.18252 |
| 9 | 1.82977 | 1.12807 | 0.22432 |
| **$S^+$** | **1.93382** | **1.24187** | **0.23547** |
| **$S^-$** | **1.20369** | **1.00242** | **0.05155** |

STEP 3
Then the PIS ($S^+$) and NIS ($S^-$) has been calculated using equation (3),

$$s^+ = \{(Max(v_{ij}) \mid j\varepsilon J^*), (Min(v_{ij}) \mid j\varepsilon J^*)\ i = 1, 2 \ldots 32\}$$
$$s^- = \{(Min(v_{ij}) \mid j\varepsilon J^*), (Max(v_{ij}) \mid j\varepsilon J^*)\ i = 1, 2 \ldots 32\} \quad (3)$$

where, $J$ is a set of beneficial attributes and $J^*$ is a set of non-beneficial attributes. The $s^+$ and $s^-$ values are shown in Table 6.

Table 7. Separation measures, Closeness coefficient value and rank

| Expt. No | $D_i^+$ | $D_i^-$ | $C_i$ | Rank |
|---|---|---|---|---|
| 1 | 6.7382E-06 | 0.790093 | 0.99999 | 1 |
| 2 | 0.76376048 | 0.111348 | 0.12723 | 9 |
| 3 | 0.24121549 | 0.580904 | 0.70659 | 6 |
| 4 | 0.22893566 | 0.56645 | 0.71217 | 5 |
| 5 | 0.11461334 | 0.689524 | 0.85747 | 2 |
| 6 | 0.29269311 | 0.513226 | 0.63682 | 7 |
| 7 | 0.19802865 | 0.604087 | 0.75311 | 4 |
| 8 | 0.32719955 | 0.529956 | 0.61827 | 8 |
| 9 | 0.15459467 | 0.661529 | 0.81057 | 3 |

STEP 4
The separation of each alternative from PIS ($S^{+)}$ and NIS ($S^-$) is found as per equation (4) and equation (5),

$$D_i^+ = \sqrt{\sum_{i=1}^{32} \left(v_{ij} - s_j^+\right)^2} \quad i = 1, 2 \cdots 32 \quad (4)$$

$$D_i^- = \sqrt{\sum_{i=1}^{32} \left(v_{ij} - s_j^-\right)^2} \quad j = 1, 2, 3 \quad (5)$$

STEP 5
The closeness coefficient value of each alternative ($C_i$) is calculated as shown in equation (6), The closeness coefficient values are shown in Table 7.

$$C_i = \frac{D_i^-}{D_i^- + D_i^+} \quad (6)$$

## 4. RESULTS AND DISCUSSIONS

From the main effects plot (shown in Fig. 5) the optimum parameters were recognized at tool rotational speed of 710 rpm, feed of 30 mm/rev, and tilt angle of 2º. The closeness coefficient increases with an increase in feed and tilt angle whereas the closeness coefficient decreased from tool rotational speed 710 rpm to 900 rpm and then the closeness coefficient increases from the tool rotational speed 900 rpm to 1120 rpm.

A higher value of closeness coefficient value indicates better performance. From Table 7, it is evident that experiment no. 1 accomplished the highest value of closeness coefficient amongst the 9 experiments and the optimum condition to achieve the multiple performance characteristics (tool rotational speed = 710 rpm, feed = 30 mm/rev, and tilt angle = 2º).
From Table 7, it is evident that experiment number 1 was the better performer. The order of the experimental run obtained by TOPSIS was given as 1-5-9-7-4-3-6-8-2.

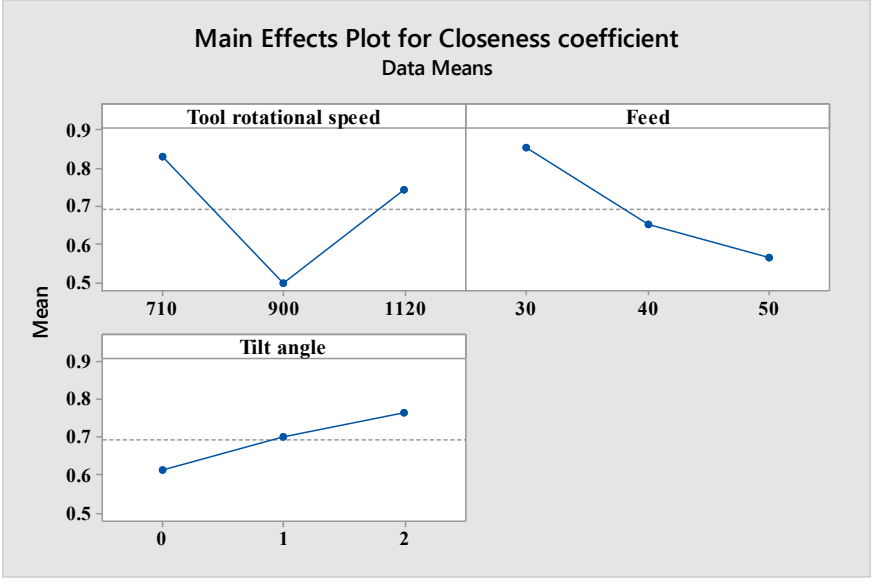


Fig. 5 Main effects plot for closeness coefficient

Tool rotational speed is given rank 1 in the mean response table (Table 8), making it the most crucial factor in determining the response, followed by feed and tilt angle. Exp. No Vs closeness coefficient is depicted in Fig. 6.

Table 8. Mean response table for Closeness coefficient value

| Level | Factor | | |
|---|---|---|---|
| | Tool rotational speed | Feed | Tilt angle |
| Level 1 | **0.831427** | **0.854561** | 0.611274 |
| Level 2 | 0.499543 | 0.653896 | 0.700703 |
| Level 3 | 0.743112 | 0.565626 | **0.762106** |
| Max-Min | 0.331884 | 0.288935 | 0.150832 |
| Rank | 1 | 2 | 3 |

Table 9. ANOVA for Closeness coefficient

| Source | DF | Seq SS | Adj SS | Adj MS | F | P | % of contribution |
|---|---|---|---|---|---|---|---|
| Tool rotational speed | 2 | 0.21885 | 0.17727 | 0.08864 | 1.42 | 0.413 | 46.75 |
| Feed | 2 | 0.17312 | 0.13154 | 0.06577 | 1.05 | 0.487 | 36.98 |
| Tilt angle | 2 | 0.05531 | 0.03452 | 0.01726 | 0.28 | 0.783 | 11.81 |
| Error | 2 | 0.02079 | 0.12475 | 0.06238 | | | 4.44 |
| Total | 8 | 0.46809 | | | | | |

S = 0.249754 R-Sq = 95.35% R-Sq(adj) = 0.00%

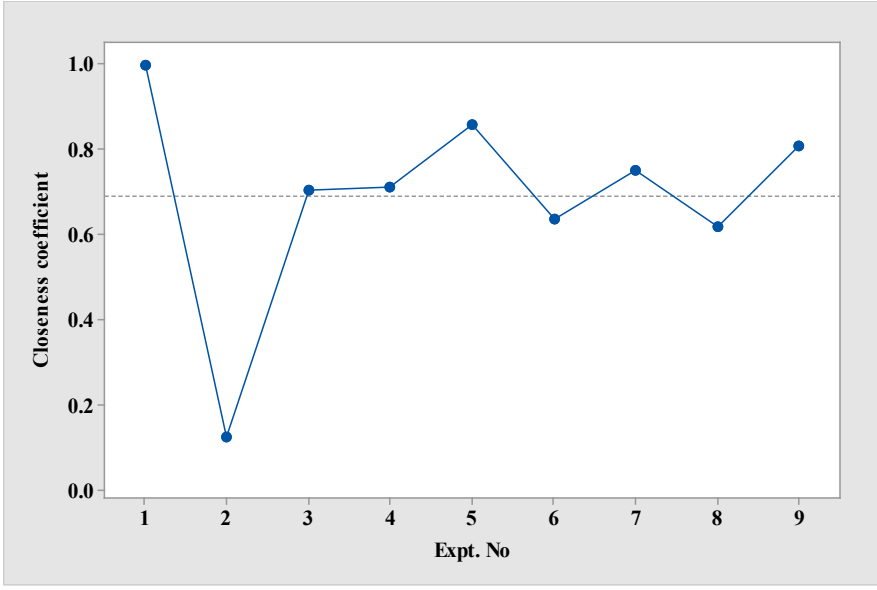


Fig. 6 Expt. No Vs closeness coefficient

ANOVA was used to estimate the percentage contribution of each process parameters on multi-objective optimization. From the ANOVA analysis, it is clear that tool rotational speed contribution is maximum (46.75%) afterward feed (36.98%), and tilt angle (11.81%) as depicted in Table 9. The regression equation for Closeness coefficient is given in equation 7.

$$\text{Closeness coefficient} = 1.36 - 0.000181 \times \text{Tool rotational speed} - 0.0144 \times \text{Feed} + 0.075 \times \text{Tilt angle} \quad (7)$$

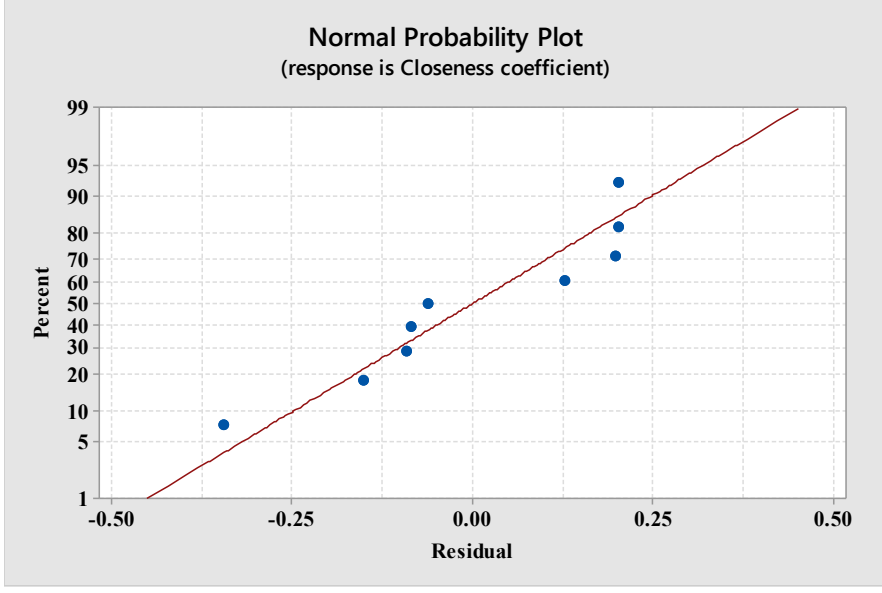


Fig. 7 Normal probability plot for residuals

The closeness coefficient for the obtained optimum combination of parameters was 1.065378 appraised from Eq. 8 and was 6.5% greater than the maximum closeness coefficient corresponding to rank 1 in Table 5.

Hence the values obtained were optimum.

$$\gamma = \gamma_m + \sum_{i=1}^{q} (\overline{\gamma_j} - \gamma_m) \tag{8}$$

The normal probability plot is presented in Fig. 7 . The errors are distributed normally because the residuals fall on a straight line [27].

In general, AA 2XXX and 7XXX alloys are employed in aircraft structures and satellite configuration.

High strength aluminium alloys are still crucial in the airframe structures. For instance, the Apollo Lunar Module's structure makes extensive use of the AA 7075 material.

## 5. CONCLUSIONS

During FSW of different AA2014-AA7075, the optimization of parameters with multiple performance characteristics (Tensile strength, Hardness, and Percentage of Elongation) was done. Tool rotational speed, feed, and tilt angle were taken into account as process parameters. The trials followed the L9 orthogonal array, and TOPSIS was used for multi-objective optimization. From this research, the following findings could be made:

- Tool rotational speed was observed to be the most significant factor affecting the responses followed by feed and tilt angle.
- It is clear from the results of TOPSIS that experiment no. 1 has the highest closeness coefficient value. The obtained optimum combinations of parameters are i.e. Tool rotational speed-710 rpm, Feed rate-30 mm/rev, and tilt angle-2$^{o}$.
- From the ANOVA tool rotational speed (46.75%) has a significant influence followed by feed (36.98%), and tilt angle (11.81%) has the least influence
- From the values of closeness coefficient, the FSW parameters best combination can be arranged in the order 1-5-9-7-4-3-6-8-2.
- The results obtained were in good agreement with ANOVA.
- An improvement of 6.5% of the predicted weighted closeness coefficient confirms the optimality of the obtained results.

## REFERENCES

[1] N. Z. Khan, A. N. Siddiquee, and Z. A. Khan, *Friction stir welding: Dissimilar aluminum alloys*, CRC Press, 2017.

[2] N. Z. Khan et al., Microstructural features of friction stir welded dissimilar Aluminium alloys AA2219-AA7475, *Materials Research Express*, vol. **5,** no. 5, pp. 056531, 2018.

[3] Z. Zhang, B. L. Xiao, and Z. Y. Ma, Influence of water cooling on microstructure and mechanical properties of friction stir welded 2014Al-T6 joints, *Materials Science Engineering A,* vol. **614,** pp. 6–15, 2014.

[4] M. Grujicic, G. Arakere, H. V. Yalavarthy, T. He, C. F. Yen, and B. A. Cheeseman, Modeling of AA5083 material-microstructure evolution during butt friction-stir welding, *Journal of Materials Engineering and Performance,* vol. **19,** no. 5, pp. 672–684, 2010.

[5] G. Çam and S. Mistikoglu, Recent developments in friction stir welding of al-Alloys, *Journal* of *Materials Engineering and Performance,* vol. **23,** no. 6, pp. 1936–1953, 2014.

[6] A. Heidarzadeh, S. Mironov, R. Kaibyshev, G. Çam, A. Simar, A. Gerlich, F. Khodabakhshi, A. Mostafaei, D. P. Field, J. D. Robson, A. Deschamps and P.J. Withers, Friction stir welding/processing of metals and

alloys: A comprehensive review on microstructural evolution., *Progress in Materials Science,* vol. **117,** 2021.
[7] N. Kashaev, V. Ventzke, and G. Çam, Prospects of laser beam welding and friction stir welding processes for aluminum airframe structural applications, *Journal of Manufacturing Processes,* vol. **36,** pp. 571-600, 2018.
[8] G. Çam and G. İpekoğlu, Recent developments in joining of aluminium alloys*, International Journal of Advanced Manufacturing Technology,* vol. **91,** no. 5-8, pp. 1851-1866, 2017.
[9] G. Çam, Friction Stir Welded Structural Materials: Beyond Al-Alloys, *International Materials Reviews*, vol. **56,** no. 1, pp. 1-48, 2011.
[10] A. Von Strombeck, G. Çam, J. F. Dos Santos, V. Ventzke, and M. Koçak, *A Comparison Between Microstructure, Properties, and Toughness Behavior of Power Beam and Friction Stir Welds in Al-Alloys*, Proc. of the TMS 2001 Annual Meeting Aluminum, Automotive and Joining (New Orleans, Louisiana, USA, February 12-14, 2001), eds: S.K. Das, J.G. Kaufman, and T.J. Lienert, pub.: TMS, Warrendale, PA, USA, pp. 249-264, 2001.
[11] G. İpekoğlu, S. Erim, and G. Çam, Investigation into the influence of post-weld heat treatment on the friction stir welded AA6061 Al-alloy plates with different temper conditions, *Metallurgical and Materials Transactions A*, vol. **45A**, no. 2, pp. 864-877, 2014.
[12] H. Robe, Y. Zedan, J. Chen, H. Monajati, E. Feulvarch, and P. Bocher, Microstructural and mechanical characterization of a dissimilar friction stir welded butt joint made of AA2024-T3 and AA2198-T3, *Materials Characterization,* vol. **110,** pp. 242–251, 2015.
[13] J. F. Guo, H. C. Chen, C. N. Sun, G. Bi, Z. Sun, and J. Wei, Friction stir welding of dissimilar materials between AA6061 and AA7075 Al alloys effects of process parameters, *Materials and Design,* vol. **56,** pp. 185–192, 2014.
[14] G. İpekoğlu and G. Çam, Effects of initial temper condition and post weld heat treatment on the properties of dissimilar friction-stir-welded joints between AA7075 and AA6061 aluminum alloys, *Metallurgical and Materials Transactions A,* vol. **45,** no. 7, pp. 3074-3087, 2014.
[15] G. Çam, G. İpekoğlu, and H.T. Serindağ, Effects of use of higher strength interlayer and external cooling on properties of friction stir welded AA6061-T6 joints, *Science and Technology* of *Welding and Joining*, vol. **19,** no. 8, pp. 715-720, 2014.
[16] C. Chanakyan, S. Sivasankar, M. Meignanamoorthy, and S. V. Alagarsamy, Parametric Optimization of Mechanical Properties via FSW on AA5052 Using Taguchi Based Grey Relational Analysis, *INCAS BULLETIN,* vol. **13,** Issue 2, pp. 21-30, https://doi.org/10.13111/2066-8201.2021.13.2.3, 2021.
[17] Nidhi Sharma, Zahid A Khan, Arshad Noor Siddiquee and Mohd Atif Wahid, Multi-response optimization of friction stir welding process parameters for dissimilar joining of Al6101 to pure copper using standard deviation based TOPSIS method, *Proc IMechE Part C: J Mechanical Engineering Science,* vol. **233,** Issue 18, pp.1–10, 2019. https://doi.org/10.1177/0954406219858628
[18] Raj Kumar, Vikas Upadhyay, and Chaitanya Sharma, Modeling and Optimization of Process Parameters For Friction Stir Welding of Dissimilar Aerospace Alloys AA2014 and AA7075, *Engineering Review,* pp.1-20, 2021.
[19] A. Farzadi, M. Bahmani, and D. F. Haghshenas, Optimization of Operational Parameters in Friction Stir Welding of AA7075-T6 Aluminum Alloy Using Response Surface Method, *Arabian Journal for Science and Engineering,* vol. **42,** pp. 4905–4916, 2017.
[20] Madhusudan Manjunath, Shridhar Umapathy Kurse, Subramanian Pillappan Shanmuganatan, and Jacob, John Investigation of effect of process parameters on friction stir welded dissimilar AA6061 T6 and AA7075 T651, *AIP Conference Proceedings,* 2236, 040002 2020, https://doi.org/10.1063/5.0006821
[21 B.Ravi Sankar, and P.Umamaheswarrao, Optimisation of hardness and tensile strength of friction stir welded AA6061 alloy using response surface methodology coupled with grey relational analysis and principle component analysis, *International Journal of Engineering, Science and Technology,* vol. **7**, no.4, pp. 21-29. 2015
[22] L. Suvarna Raju, Borigorla Venu, G. Mallaiah, Multi objective optimization of process parameters of AA2014 Friction Stir Weldments using Genetic Algorithm, *INCAS BULLETIN*, Vol. **12**, Issue 3, pp. 183-193, https://doi.org/10.13111/2066-8201.2020.12.3.15, 2020.
[23] B.Ravi Sankar, and P.Umamaheswarrao, Modelling and Optimisation of Friction Stir Welding on AA6061 Alloy, *Materials Today: Proceedings,* vol. **4,** pp.7448–7456, 2017.
[24] Janusz Torzewski, Magdalena Łazi´nska, Krzysztof Grzelak, Ireneusz Szachogłuchowicz and Janusz Mierzy´nski Microstructure and Mechanical Properties of Dissimilar Friction Stir Welded Joint AA7020/AA5083 with Different Joining Parameters, *Materials,* vol. **15,** 1910. pp. 1-16, 2022. https://doi.org/10.3390/ma15051910

[25] Yoon K. Paul, and Ching-Lai Hwang, *Multiple attribute decision making: an introduction*, Vol. **104**, Sage Publications, 1995.

[26] Shojaeefard, Mohammad Hasan, Mostafa Akbari and Parviz Asadi, Multi objective optimization of friction stir welding parameters using FEM and neural network, *International Journal of Precision Engineering and Manufacturing,* vol. **15,** no. 11, pp. 2351-2356, 2014.

[27] D. I. Lalwani, N. K. Mehta and P. K. Jain, Experimental investigations of cutting parameters influence on cutting forces and surface roughness in finish hard turning of MDN250 steel, *Journal of Materials Processing Technology,* vol. **206,** no. 1–3, pp.167–179, 2008.